Project 2 – VLM

Ty Brown

Introduction

Vortex Lattice Method (VLM) is a relatively simple yet effective tool for examining the characteristics of a finite wing. VLM is especially applicable in the early stages of wing design and development. This method is essentially a three-dimensional extension to thin airfoil theory. VLM is based on the concept that a lifting surface can be approximated by a collection of horseshoe vortices, arranged in a lattice pattern over discrete panels [1].

VLM relies on several key assumptions to provide valuable lifting surface data. One assumption is that the surface is defined as a thin airfoil. This includes the assumption of potential flow, meaning the flow is irrotational, incompressible and inviscid [2]. We also impose the Kutta condition to ensure smooth airflow at the trailing edge. Additionally, the no-flow-through condition is applied at select control points, typically located at the ¾-chord point of each panel [1].

As stated prior, the lifting surface is evaluated by using a series of horseshoe vortices arranged on a lattice of panels. Each of these horseshoe vortices has a bound vortex along the quarter chord of the panel and two trailing vortices are assumed to extend downstream infinitely [1]. This is shown in Figure 1. Using the Biot-Savart law, we are able to calculate the influence of each vortex panel on every other vortex panel through the resolution of a linear system of equations [3]. Once the vortex strengths are known, the lift distribution can be calculated using the Kutta-Juokowski theorem.

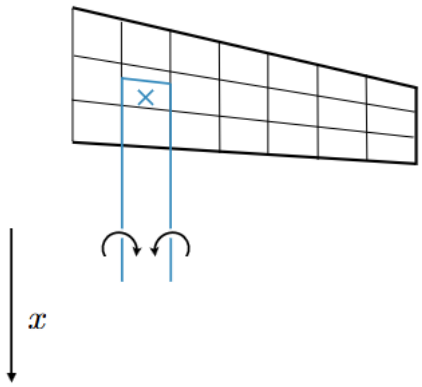

Figure 1: Example of a horseshoe vortex on a paneled lifting surface

This study focuses on exploring several aerodynamic properties, as well as an evaluation of the limitations of VLM. The effects of wing lift distribution on wing efficiency were evaluated, along with the impact of tail volume ratios on stability derivatives. The relationship between angle of attack and the lift coefficient was analyzed, which also revealed several limitations to the VLM.

Methods

For this experiment, the VortexLattice.jl library was used. This library is a "comprehensive pure-Julia implementation of the vortex lattice method for both steady and unsteady flow conditions" [4]. This library was used to perform aerodynamic analysis on finite wings and tails. The package Plots.jl was also employed to plot the resulting numerical data from Xfoil.jl [5]. This allows for a visual display of

results and a more comprehensive interpretation of the resulting data. All experimentation was completed using the Julia coding language.

The first experiment was focused on evaluating the effects of lift distribution on wing efficiency. To accomplish this, a function was written that used the root chord and number of spanwise panels to define the chord distribution as an ellipse. The distribution was mirrored to provide the full profile of a wing. The wing distribution can be seen in Figure 2. As the number of spanwise panels increased, the wing distribution increasingly more accurately matched the profile of an ellipse. This function returns its geometric values to be evaluated by a VLM solver.

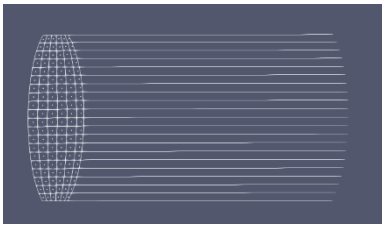

Figure 2: Elliptical wing distribution as defined by chord and spanwise panels, example defined as having 10 spanwise panels (the results were mirrored, resulting in a total of 20 panels)

To compare the effects of lift distribution on wing efficiency, the number of spanwise panels was varied in the range of 3 to 60. Values below 3 were not used to avoid computational errors. The aerodynamic efficiency ($\frac{C_L}{C_D}$) was evaluated iteratively for each wing distribution with a unique number of spanwise panels in the defined range. The resulting data comparing aerodynamic efficiency to the number of spanwise panels was plotted.

The VortexLattice.jl library was used again to evaluate the effects of vertical and horizontal tail volume ratios on the important stability derivatives of an airframe. This evaluation was completed by writing a VLM program with a wing, horizontal tail, and vertical tail. Each of these elements were defined as rectangles having no twist, no dihedral, and no sweep. Each element was defined to have the same chord for simplicity. In addition, both tails were defined as having their quarter-chord point 4.0 units behind the quarter-chord point of the wing. This geometry definition can be seen in Figure 3.

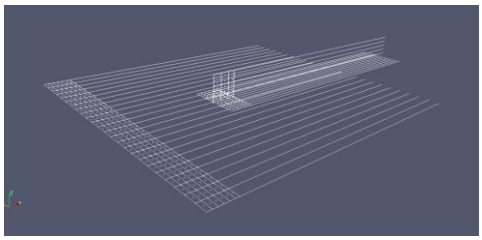

Figure 3: Defined wing/tail combination used for VLM calculations

The equations for the horizontal tail volume ratio (Eq 1) and vertical tail volume ratio (Eq 2) are defined as follows:

$$V_h = \frac{S_h x_h}{S_w c_w} \qquad [1]$$

$$V_v = \frac{S_v x_v}{S_w b_w} \qquad [2]$$

where S_h is the horizontal tail area, x_h is the length between the aerodynamic centers of the wing and horizontal tail, S_w is the wing area, and c_w is the mean aerodynamic chord of the wing in Eq 1. In Eq 2, S_v is the vertical tail area, x_v is the length between the aerodynamic centers of the wing and vertical tail, S_w is again the wing area, and b_w is the wing span.

The span of both the horizontal and vertical tails were independently varied in a range of .2 to 1.6. The tail not being evaluated was

considered to have a constant span of 1.0. Calculations for the horizontal tail volume ratio and the vertical tail volume ratio were completed for each value in the range. In addition, the longitudinal static stability, yaw static stability, and roll static stability derivatives were all computed using the VLM.

Results were pushed into different arrays. The Plots.jl library was the used to plot the various static stability derivatives against the corresponding tail volume ratios.

The effects of angle of attack on the lift coefficient were also evaluated. This experiment was completed using a wing defined as having no twist, no dihedral, and moderate sweep (Figure 4). The angle of attack was adjusted iteratively, then plotted to evaluate the resulting coefficient of lift.

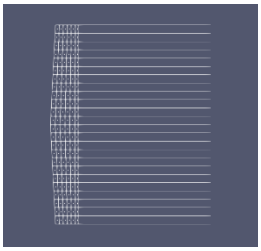

Figure 4: Wing distribution used to analyze effects of angle of attack

Results and Discussion

The variation of lift distribution to evaluate the resulting wing efficiency yielded data that shows a distinct trend. Figure 4 shows that as the number of spanwise panels increased, the wing efficiency increased also. This occurs at a rapid rate initially but eventually stabilizes relatively. The efficiency reaches a maximum of approximately 29.3 when the lift distribution is defined by 100 spanwise sections.

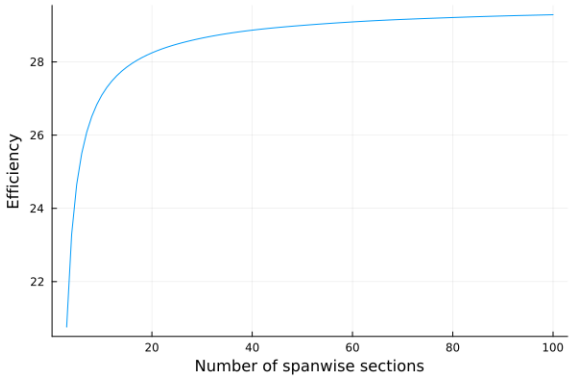

Figure 5: Wing efficiency versus number of spanwise sections

This indicates that as the lift distribution approaches an elliptical distribution, the wing efficiency increases. Figure 6 and Figure 7 shows how the wing distribution approaches an ellipse as the number of spanwise panels increases. An elliptical profile is the most efficient for a lift distribution [1]. The data collected from this experiment supports that fact.

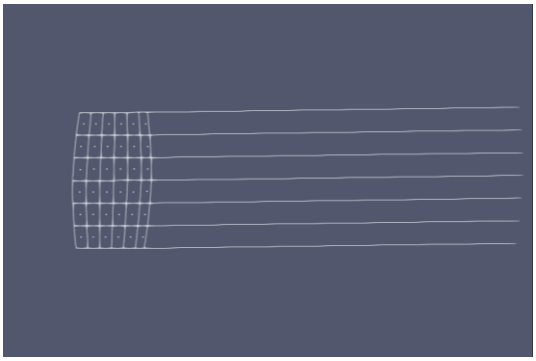

Figure 6: Wing distribution for panel number defined as 3

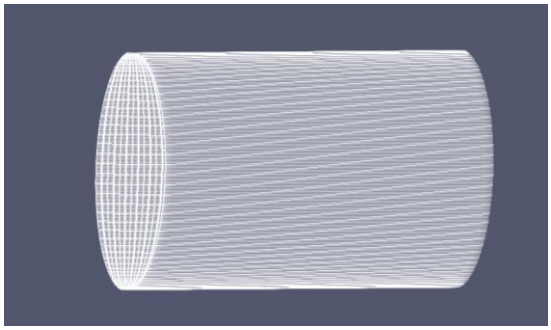

Figure 7: Wing distribution for panel number defined as 100

The effect of tail volume ratios on the various stability derivatives was measured. There were distinct trends for each stability derivative when varying both horizontal and vertical tail volume coefficients.

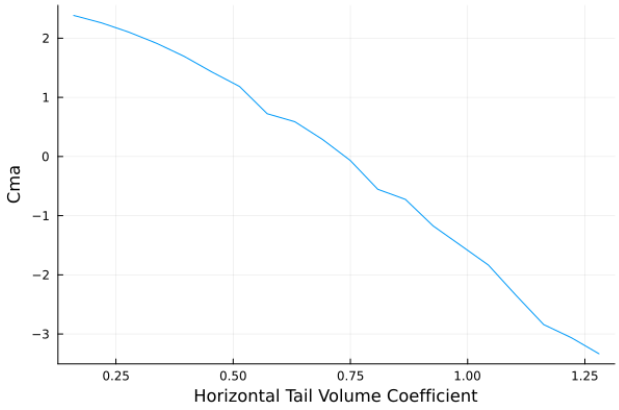

Figure 8: Longitudinal Static Stability Derivative (Cma) vs Horizontal Tail Volume Coefficient

Figure 8 indicates that the longitudinal static stability derivative has a near linear decrease as the horizontal tail volume coefficient increases. To produce a stable aircraft, a negative longitudinal static stability derivative is desirable [6]. A negative value ensures that the aircraft generates a restoring moment back to the equilibrium position when the aircraft experiences nose-up motion. This restoring moment prevents excessive upwards pitch and reduces the risk of stall.

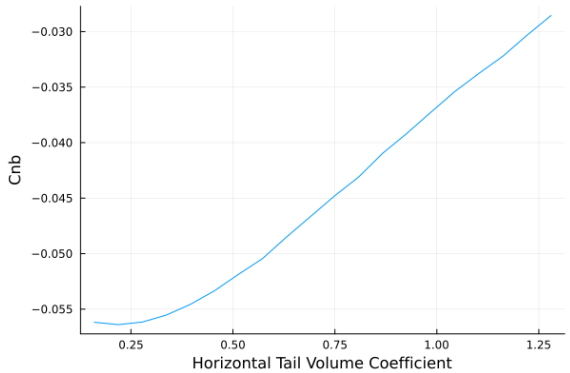

Figure 9: Yaw Static Stability Derivative (Cnb) vs Horizontal Tail Volume Coefficient

As seen in Figure 9, the horizontal tail volume coefficient has a minor impact on the yaw stability derivative. This is intuitive because yaw is related more to a vertical tail. Yaw stability will be discussed further in a later section.

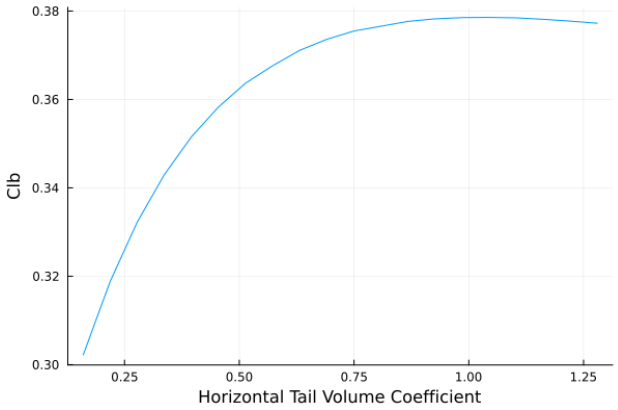

Figure 10: Roll Static Stability Derivative (Clb) vs Horizontal Tail Volume Coefficient

The roll static stability is positive and generally increasing with horizontal tail volume coefficient in Figure 10. This is not ideal for stability; roll stability should be a negative value to create a counteracting moment to roll motion, which restores equilibrium. Roll stability is most effected by dihedral. [6] Both the wing and horizontal tail do not have dihedral in this VLM simulation, and thus they do not produce an ideal roll stability derivative.

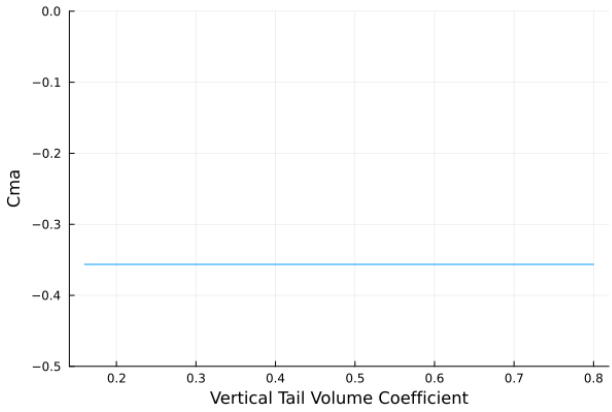

Figure 11: Longitudinal Static Stability Derivative (Cma) vs Vertical Tail Volume Coefficient

Figure 11 shows that varying the vertical tail volume coefficient has no effects on the longitudinal static stability derivative of an aircraft. This is a logical conclusion, as this derivative relates to pitch. The vertical tail will have no impact in this plane of rotation.

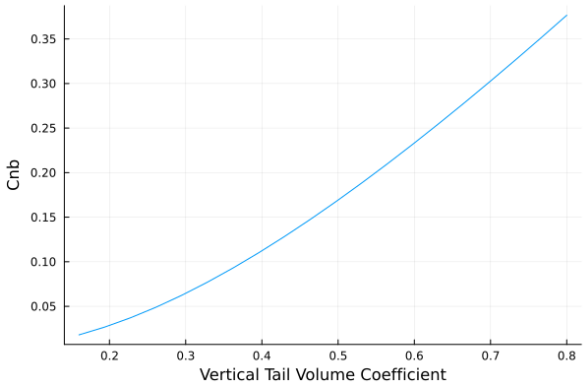

Figure 12: Yaw Static Stability Derivative (Cnb) vs Vertical Tail Volume Coefficient

As the vertical tail volume coefficient increases, the yaw stability derivative also increases. This is ideal, as a positive yaw static stability derivative is necessary for a stable aircraft [6]. The vertical wing produces a side force to counteract sideslip. A larger vertical area increases the restoring moment in the yaw direction.

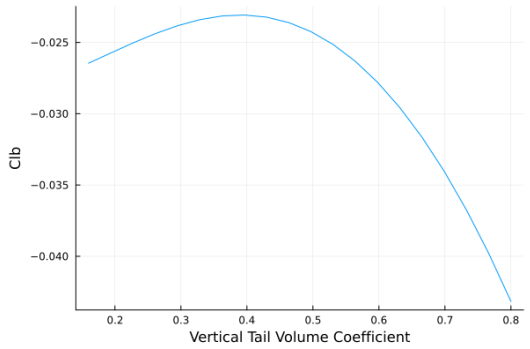

Figure 13: Roll Static Stability Derivative (Clb) vs Vertical Tail Volume Coefficient

There is very little relationship between the vertical tail volume coefficient and the roll static stability. Once again, this value is largely affected by dihedral rather than either vertical or horizontal tail volume coefficients.

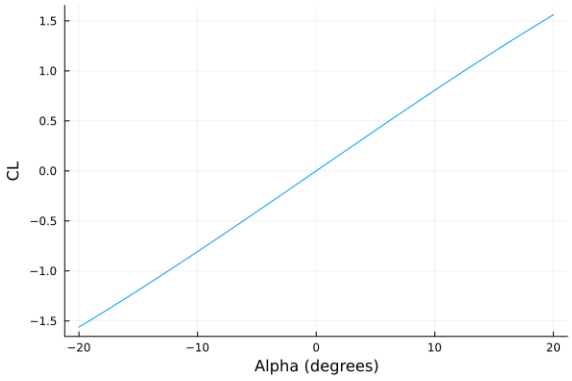

Figure 14: Angle of Attack (Alpha) vs Coefficient of Lift (CL)

Varying the angle of attack on a constant wing shape resulted in the lift coefficient pattern viewed in Figure 14. This reveals limitations to VLM. We see that VLM does not predict stall. This is due to the fact that VLM does not account for boundary layers or viscous effects. Because of this, VLM cannot predict flow separation, and therefore VLM can also not predict the onset of stall.

References

1. Ning, Andrew. *Computational Aerodynamics*. First electronic edition. 2020.

2. 2.016 hydrodynamics fluid forces on bodies. Accessed March 21, 2025. https://web.mit.edu/2.016/www/handouts/2005Reading5.pdf.

3. Aerodynamics of 3D Lifting Surfaces through Vortex Lattice Methods. https://archive.aoe.vt.edu/mason/Mason_f/CAtxtChap6.pdf.

4. VortexLattice.jl. https://flow.byu.edu/VortexLattice.jl/stable/guide/.

5. JuliaPlots/Plots.Jl. 2015. JuliaPlots, 31 Jan. 2025. GitHub

6. Ning, Andrew. *Flight Vehicle Design*. First electronic edition. 2018